Unified model-independent *S*-matrix description of nuclear rainbow, prerainbow, and anomalous large-angle scattering in ^{4}He-^{40}Ca elastic scattering

V. Yu. Korda,[1,*] A. S. Molev,[1] V. F. Klepikov,[1] and L. P. Korda[1,2]

[1]*Institute of Electrophysics and Radiation Technologies, National Academy of Sciences of Ukraine, 28 Chernyshevsky Street, Post Office Box 8812, UA-61002 Kharkov, Ukraine*

[2]*NSC Kharkov Institute of Physics and Technology, National Academy of Sciences of Ukraine, 1 Akademicheskaya Street, UA-61108 Kharkov, Ukraine*

(Received 14 January 2015; revised manuscript received 10 February 2015; published 27 February 2015)

Using the evolutionary model-independent *S*-matrix approach, we show that a simultaneous correct description of the pictures of nuclear rainbow, prerainbow, and anomalous large-angle scattering (ALAS) in the ^{4}He-^{40}Ca elastic scattering can be achieved with help of the *S*-matrix moduli and the real nuclear phases exhibiting smooth monotonic dependencies on angular momentum, while the quantum deflection functions have a form characteristic of the nuclear rainbow case. The special role of the surface partial waves in the formation of ALAS is revealed.

DOI: 10.1103/PhysRevC.91.024619 PACS number(s): 24.10.Ht, 25.70.Bc

I. INTRODUCTION

The elastic scattering of α particles by nuclei with mass numbers $A \leqslant 40$ at $E \approx 5$–25 MeV/nucleon shows a variety of scattering pictures. At $E \geqslant 20$ MeV/nucleon the nuclear rainbow picture with the characteristic wide maximum followed by the regular falloff of the differential cross section is observed (see, e.g., Refs. [1–3]). As the energy decreases, the prerainbow scattering picture with various interference structures (e.g., Airy structures of different order) and the violation of the regular falloff of the differential cross section appear (see, e.g., Refs. [4,5]). At lower energies the anomalous large angle scattering (ALAS) picture, mostly pronounced in the scattering on the nuclei with equal numbers of protons and neutrons, with the unusual enhancement (by the order of magnitude and more) of the oscillating cross section in the region of large angles comes into play (see, e.g., Refs. [6–8]).

This variety of the scattering pictures makes a problem for their valid theoretical description. The mentioned picture of nuclear rainbow is usually reproduced with help of the simple physically reasonable model representation for the nuclear part of the scattering matrix in the space of angular momentum l. The respective modulus and real nuclear phase, being smooth monotonic functions of l, correctly account for the gradual elimination of the partial waves from the incoming wave and the change of refraction in the nuclear matter (see, e.g., Refs. [9–11]). To describe the more complicated scattering pictures (like prerainbow and ALAS), the mentioned simple (background) model scattering matrix has to be modified by the additional corrections (the resonance-like pole terms [12–14], the small fluctuations of scattering matrix [15], etc.) that violate the smooth and monotonic behavior of the modulus and the real nuclear phase in the angular momentum space. The behavior of the modulus and the real nuclear phase extracted from various optical nucleus–nucleus potentials that replicate the mentioned scattering pictures also appears nonmonotonic, in particular, due to the presence of nonsmooth structures (see, e.g., Refs. [8,15–20]).

Thus, there arises the question of whether it is possible to build the unified description of all the scattering pictures that exist at the considered energies (from the nuclear rainbow at sufficiently high energies to the ALAS at the lower energies) with the use of conventional smooth monotonic representations for the scattering matrix modulus and nuclear phase. To answer the question, we apply the evolutionary model-independent *S*-matrix approach [21], which has proved very efficient not only for the analysis of the nuclear rainbow picture [22] but also for the study of the more complicated refractive scattering patterns with the prerainbow oscillations [23]. In the present paper we apply this approach to describe the evolution of the observed scattering pictures in the system ^{4}He+^{40}Ca at 7–21 MeV/nucleon. Experimental data are from Refs. [24–26].

II. CALCULATION PROCEDURE

In our approach, the scattering matrix that describes the ^{4}He-^{40}Ca elastic scattering has the form $S(l) = S_N(l) \exp[2i\sigma_C(l)]$, where $S_N(l) = \eta(l) \exp[2i\delta_r(l)]$ is the nuclear part, $\sigma_C(l)$ is the Coulomb scattering phase taken to be the quasiclassical phase of the point-charge scattering by the uniformly charged sphere (see, e.g., Ref. [10]) having the radius $R_C = 1.3 \times 40^{1/3}$ [6,15], $\eta(l) = \exp[-2\delta_a(l)]$ is the scattering matrix modulus, $\delta_r(l)$ is the nuclear refraction phase (real part of the nuclear phase), and $\delta_a(l)$ is the nuclear absorption phase (imaginary part of the nuclear phase). The calculations are made using the expansion of the scattering amplitude into a series of Legendre polynomials. The elastic scattering differential cross section equals the squared modulus of this amplitude. The quality of the fit of the calculated differential cross section to the experimentally measured one is assessed by means of the standard χ^2 magnitude per datum. The experimental errors are assumed to be equally weighted (10% error bars) (e.g., Refs. [15,22]). The necessary monotonicity and smoothness of the phases $\delta_{a,r}$ as functions of l are achieved with help of the restrictions imposed on

*Corresponding author: kvyu@kipt.kharkov.ua

the behavior of the first few derivatives of these phases [21]. Detailed description of the numerical procedure that helps to extract the functions $\delta_{a,r}(l)$ from the experimental data is given in Ref. [27].

Our evolutionary approach gives good quantitative description of the data with the nuclear rainbow and prerainbow scattering pictures and satisfactorily replicates the data with ALAS. To improve the quality of fit in the latter case, we have to soften the restrictions imposed on the behavior of derivatives of the phases $\delta_{a,r}(l)$, keeping their monotonicity and smoothness. If we remove all the mentioned restrictions, then we obtain better quality of fit but permit the nonmonotonic structures in $\eta(l)$ and $\delta_r(l)$ to appear. However, the nonmonotonic structures that arise in $\eta(l)$ and $\delta_r(l)$ in this case appear quite different from run to run of the fitting procedure and from the structures obtained within the optical model calculations [8,16,19] and the other S-matrix approaches (e.g., Ref. [15]). Obviously, if and only if the same nonmonotonic structures repeatedly appear in the scattering matrix alongside with the substantial improvement in the quality of fit, then one should admit that the existence of these structures is physically motivated and the search for their physical interpretation is justified.

Note that we do not explicitly consider the contribution of the processes that cannot be distinguished from the elastic scattering (e.g., the elastic α-particle transfer that can influence the formation of ALAS picture [28,29]) but further suppose that even if such processes do take place their contribution is reflected in the behavior of the scattering matrix extracted from the data.

More detailed analysis of refractive and diffractive features of the structures inherent in the elastic scattering cross sections under discussion at midangles and large angles can be performed with help of the nearside-farside decomposition [30]. To identify the Airy structures we use both the farside component and the farside component calculated without absorption in the scattering matrix [$\eta(l) = 1$ for all l] (see, e.g., Refs. [1,2,18,31]).

III. RESULTS OF CALCULATIONS AND THEIR DISCUSSION

The scattering matrices for the ^{4}He-^{40}Ca elastic scattering at $E = 29$–82 MeV found with help of our approach are shown in Figs. 1(a) and 1(b). Figure 1(c) presents the quantum deflection

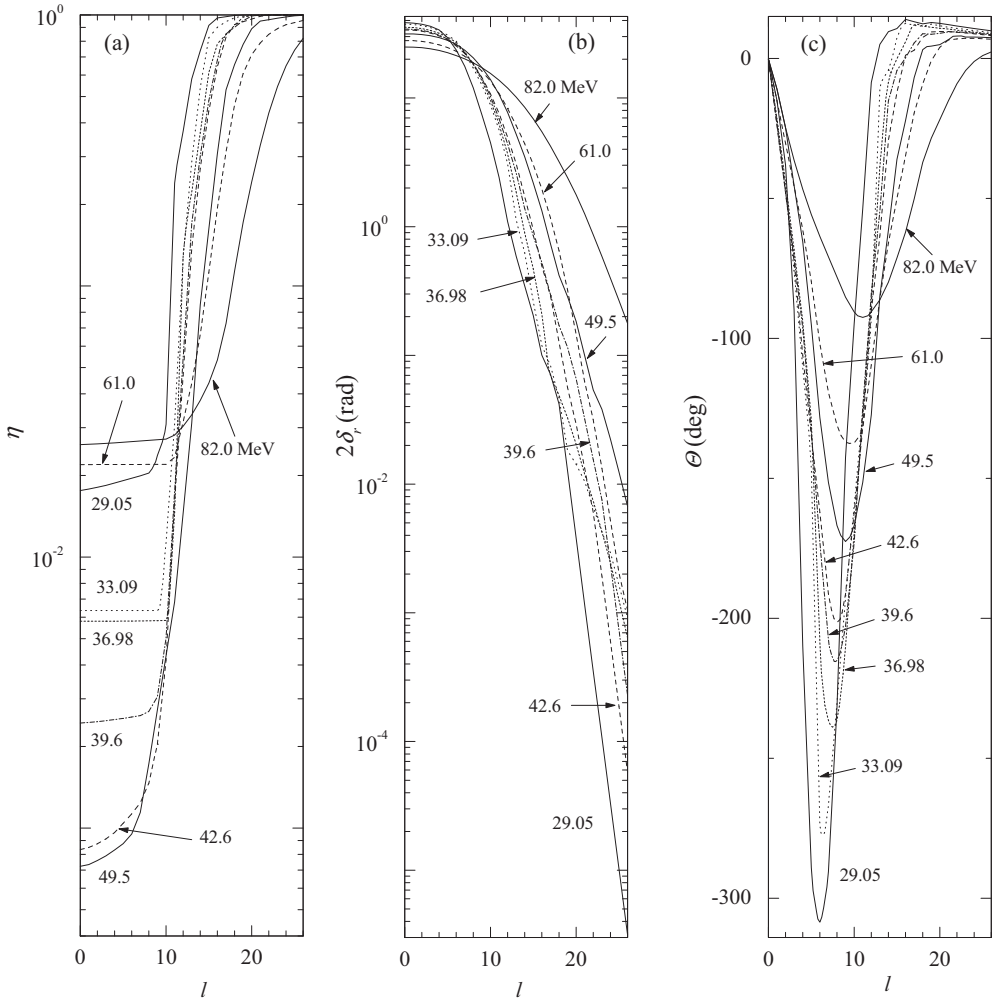

FIG. 1. (a) Scattering matrix moduli $\eta(l)$, (b) nuclear phases $\delta_r(l)$, and (c) deflection functions $\Theta(l)$ for the ^{4}He-^{40}Ca elastic scattering at $E = 29.05$–82.0 MeV.

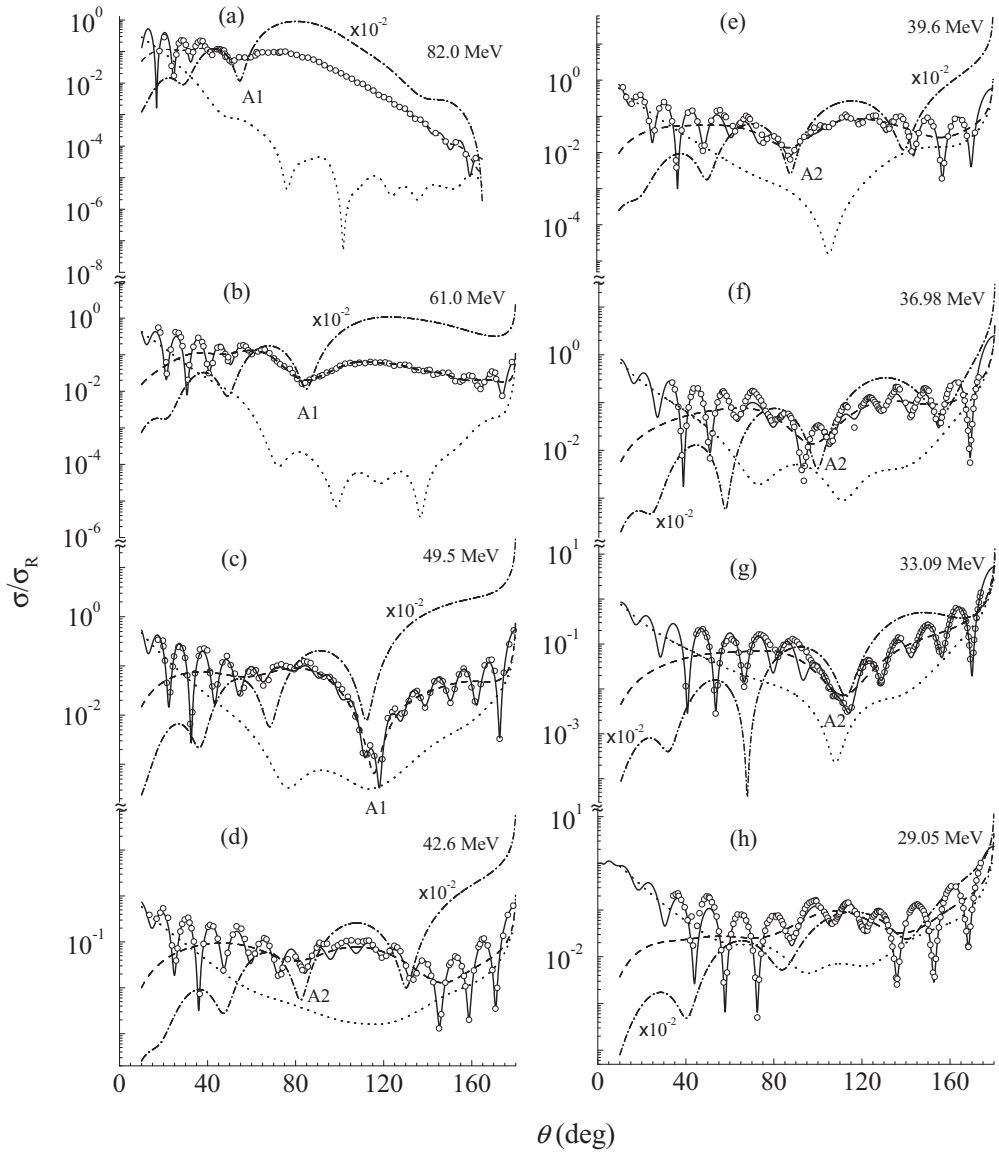

FIG. 2. (a)–(h) Elastic scattering differential cross sections (ratio to Rutherford) for the system ^{4}He+^{40}Ca at $E = 29.05$–82.0 MeV (solid curves), their farside (dashed curves) and nearside (dotted curves) components, and farside cross-section components calculated without absorption in the scattering matrix (dash-dotted curves). $A1$ and $A2$ denote the Airy minima of first and second orders. The data are from Refs. [24–26].

functions $\Theta(l) = 2d\left[\delta_r(l) + \sigma_C(l)\right]/dl$. In each case under investigation, from the nuclear rainbow at sufficiently high energies to the ALAS at the lower energies, the data in the whole angular range considered are correctly described by the differential cross section (Fig. 2) calculated with the obtained smooth monotonic representations for the scattering matrix modulus and nuclear phase (Fig. 1). The evolution with energy of the values of the nuclear transparency $\eta(0)$, the intensity of nuclear refraction $2\delta_r(0)$, the strong absorption angular momentum $l_{s.a.}$ defined by the correlation $1 - \eta^2(l_{s.a.}) = 0.5$, the nuclear rainbow angle θ_R [which corresponds to the minimum of the deflection function $\Theta(l)$], the total reaction cross section σ_R^t, and χ^2/N (N is the number of experimental points) for the calculated cross sections is presented in Table I.

The transition from the picture of nuclear rainbow ($E = 82.0$ MeV) to the picture of ALAS ($E = 49.5$ MeV) is accompanied by the decrease of the value of the nuclear transparency $\eta(0)$ by more than the order of magnitude. Then, with further decrease of energy, $\eta(0)$ increases almost to 0.02 at $E = 29.05$ MeV. This contradicts the observation of Refs. [8,16,20] that in the case of ALAS the nuclear transparency turns out to be of the order of 0.1. The value of the nuclear refraction $2\delta_r(0)$ shows gradual increase with the decrease of energy. The quantum deflection function $\Theta(l)$ in the region $E = 29$–82 MeV is typical of the case of nuclear rainbow. With the decrease of energy, its form in the vicinity of a minimum becomes more narrow but remains mostly symmetric, contrary to the pronounced asymmetry of the form

TABLE I. Evolution with energy of the values of the nuclear transparency $\eta(0)$, the intensity of nuclear refraction $2\delta_r(0)$, the strong absorption angular momentum $l_{s.a.}$, the nuclear rainbow angle θ_R, the total reaction cross section σ_R^t, and the χ^2/N magnitude for the calculated cross sections.

E (MeV)	$\eta(0)$	$2\delta_r(0)$ (rad)	$l_{s.a.}$	θ_R (deg)	σ_R^t (mb)	χ^2/N
82.00	2.60×10^{-2}	24.88	24.6	93	1556	1.1
61.00	2.19×10^{-2}	27.93	19.9	137	1484	2.0
49.50	7.23×10^{-4}	31.49	18.4	173	1478	2.6
42.60	8.34×10^{-4}	33.76	16.5	201	1359	2.8
39.60	2.44×10^{-3}	34.32	16.1	215	1425	2.9
36.98	5.80×10^{-3}	35.40	15.6	239	1448	2.9
33.09	6.35×10^{-3}	37.40	14.6	277	1441	3.4
29.05	1.76×10^{-2}	38.47	13.8	308	1391	2.9

of deflection function typical of the optical model calculations [17,18].

We have successfully identified the Airy minima of the first $A1$ and the second $A2$ orders in the region $E =$ 33.1–82.0 MeV (Fig. 2). At $E = 29.05$ MeV the form of the angular distribution of the cross section becomes so complicated that the identification of Airy minima becomes difficult. The angular positions of the identified Airy minima $A1$ and $A2$ obey the law of the reciprocal c.m. energy dependence (Fig. 3). The discussion of this dependence can be found in Refs. [31–33]. The nuclear rainbow angle θ_R obeys the same energy dependence (Fig. 3). The use of the energy systematics shown in Fig. 3 gives a possibility of resolving the Airy ambiguity (rainbow-shift ambiguity [34]) in the analyzed cases of the ^{4}He-^{40}Ca elastic scattering.

The characteristic structures in the measured cross sections of the ^{4}He-^{40}Ca elastic scattering, that we have identified as the Airy minima $A1$ and $A2$, are also reproduced by the widely used optical model potential from Ref. [6]. However, they are differently interpreted because of the appearance of the interference Airy-like structures (see, e.g., Refs. [1,35,36]).

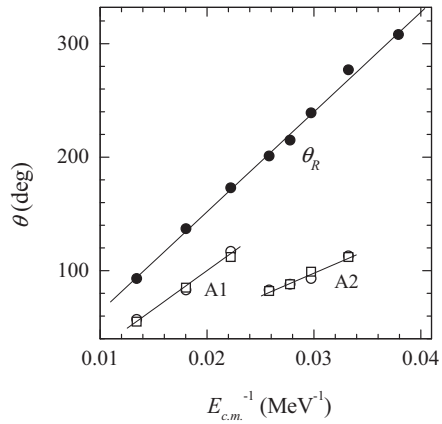

FIG. 3. Evolution with energy of the angular position of the Airy minima of first $A1$ and second $A2$ orders in the measured differential cross sections for the system ^{4}He+^{40}Ca (open circles) and in the farside cross-section components calculated without absorption in the scattering matrix (squares), and the same evolution of the nuclear rainbow angle θ_R (solid circles). Straight lines show results of fitting to the data indicated as circles.

The presence of Airy minima of definite order in the studied differential cross sections of the ^{4}He-^{40}Ca elastic scattering and the form of the deflection functions in the considered energy range stand for the "rainbow" interpretation of the data, in particular for the appearance of the ALAS picture as a consequence of the "sliding rainbow" [37] characterized by the shift of the nuclear rainbow angle beyond -180° at $E \leqslant 47$ MeV (Fig. 3). Unfortunately, we have not achieved good replication of the existing data at $E < 29$ MeV [26,38], keeping the form of the nuclear deflection function typical of the nuclear rainbow case and the restrictions imposed on the behavior of the phases $\delta_{a,r}(l)$ (see Sec. II). Thus, with further decrease of energy, our systematics and its interpretation could appear no longer valid, but we leave this problem for separate detailed investigation.

At $E = 29.05$–49.50 MeV, for each of the analyzed cross sections at very large scattering angles, we observe the moderate growth of the dominating farside cross-section component (the expression of refractive effects) and the sharp growth of the nearside component, so that their interference produces the ALAS pattern (Fig. 2).

IV. ANALYSIS OF ALAS FORMATION

Let us specify the particular partial waves that contribute to the formation of ALAS. To do that, we manually replace the original experimental data, in which the enhancement of the oscillating differential cross section is observed at large angles, by the artificial data that do not exhibit such enhancement. Then we proceed with our evolutionary calculations using the artificial data but starting from the scattering matrix extracted from the original data. When the minimum of the χ^2 magnitude is achieved we compare the scattering matrix evolved in such a manner with the one extracted from the original data. In all the ALAS cases studied, we have found that the major differences between the scattering matrix that does produce ALAS in the calculated elastic scattering differential cross section and the one that does not are concentrated in the l region around and well below the strong absorption angular momentum $l_{s.a.}$. Thus, we further gradually reduce the region of angular momenta Δl where our evolutionary approach changes the scattering matrix and then repeat calculations.

Figure 4 and Table II present some of our results obtained in such a way. Figures 4(a)–4(c) show the differences $\Delta\eta(l)$ $[\Delta\delta_r(l)]$ between the scattering matrix modulus (the nuclear phase) extracted from the original data (same as in Fig. 1) and the results of its evolution caused by the artificial data. The dashed, dotted, and dash-dotted curves are obtained for $\Delta l = \Delta l_1, \Delta l_2$, and Δl_3, respectively (Table II). We emphasize that, in spite of the nonsmooth behavior of $\Delta\eta(l)$ and $\Delta\delta_r(l)$, the evolved S-matrix moduli and nuclear phases are smooth monotonic functions of l, as specified in Sec. II. Figures 4(d)–4(f) show the differential cross sections calculated with the evolved scattering matrices. The solid curves are the same

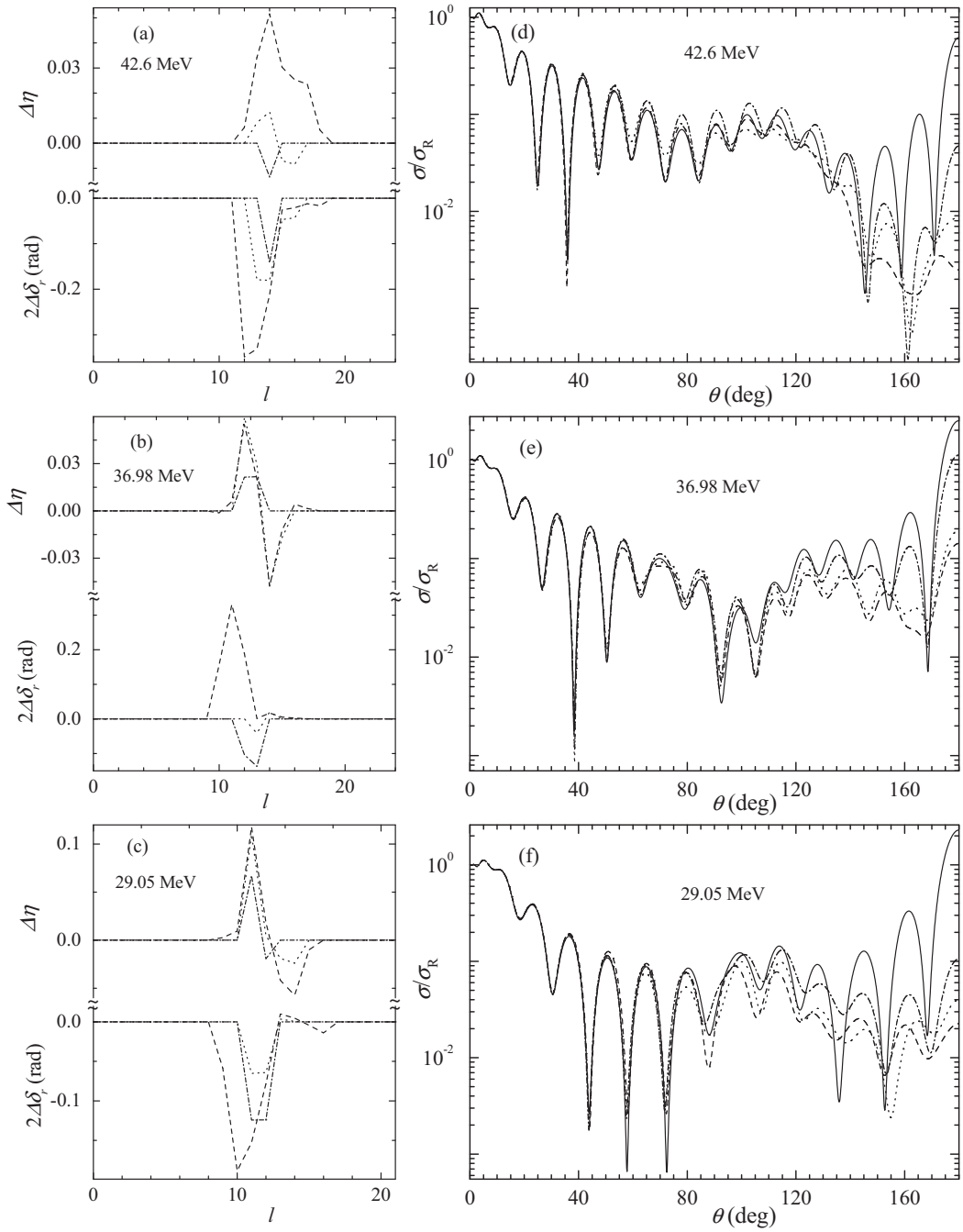

FIG. 4. Analysis of ALAS formation in the system ^{4}He+^{40}Ca at $E = 42.6$, 36.98, and 29.05 MeV. (a)–(c) Differencies $\Delta\eta\,(l)$ [$\Delta\delta_r\,(l)$] between the scattering matrix modulus (the nuclear phase) extracted from the original data (same as in Fig. 1) and the results of its evolution caused by the artificial data that do not contain ALAS. The regions of angular momenta Δl where our evolutionary approach has changed the scattering matrix are Δl_1 for dashed curves, Δl_2 for dotted curves, and Δl_3 for dash-dotted curves (Table II). (d)–(f) Elastic scattering differential cross sections (ratio to Rutherford). Solid curves are the same as in Fig. 2. Dashed, dotted, and dash-dotted curves are calculated with the scattering matrices depicted (in the form of differences) in Figs. 4(a)–4(c) (types of curves correspond).

as in Fig. 2. The dashed, dotted, and dash-dotted curves are calculated with the scattering matrices depicted (in the form of differences) in Figs. 4(a)–4(c) (types of curves correspond). This analysis reveals the special role of the surface partial waves in the formation of ALAS, which was pointed out earlier, e.g., in Refs. [19,39–42]. Note that this conclusion is a common feature of various theoretical interpretations of ALAS. In case of the use of the barrier-wave–internal-wave decomposition of the elastic scattering amplitude [43], performed within the optical model calculations, the ALAS is dominated by the internal-wave component (see, e.g., Refs. [8,20,44,45]). But the decomposition of the latter into partial amplitudes shows that ALAS appears exactly due to the contribution of several surface partial waves (e.g., Refs. [41,46]).

TABLE II. Regions of angular momenta Δl where our evolutionary approach has changed the scattering matrix.

E (MeV)	Δl_1	Δl_2	Δl_3
42.60	12–18	13–16	14
36.98	10–17	12–15	12–13
29.05	9–16	11–14	11–12

V. CONCLUSION

Using the evolutionary model-independent S-matrix approach, we have shown that a simultaneous correct description of the pictures of nuclear rainbow, prerainbow, and ALAS in the ^{4}He-^{40}Ca elastic scattering can be achieved with help of the S-matrix moduli and the real nuclear phases exhibiting smooth monotonic dependencies on angular momentum. The quantum deflection functions have a form characteristic of the nuclear rainbow case and are mostly symmetric in the vicinity of a minimum. The scattering matrix and the quantum deflection function for the system ^{4}He+^{40}Ca at $E = 29.05$–82.0 MeV show smooth physically motivated variations with the collision energy.

The Airy minima of first and second orders have been successfully identified in the differential cross sections of the ^{4}He-^{40}Ca elastic scattering. Their angular positions obey the law of the reciprocal c.m. energy dependence, which is in conformity with the rainbow interpretation of the data. The use of this energy systematics has allowed us to get rid of the rainbow-shift ambiguity and, thus, to determine the nuclear part of the scattering matrix more reliably.

We have revealed the special role of the surface partial waves in the formation of ALAS picture.

The joint study of the features of the rainbow and prerainbow scattering, and the ALAS effect in the system ^{4}He+^{40}Ca, with help of the unified model-independent S-matrix approach, has enabled us to obtain more detailed reliable information about the interaction of colliding nuclei.

[1] M. E. Brandan and G. R. Satchler, Phys. Rep. **285**, 143 (1997).
[2] D. T. Khoa, W. von Oertzen, H. G. Bohlen, and S. Ohkubo, J. Phys. G **34**, R111 (2007).
[3] M. E. Brandan, M. S. Hussein, K. W. McVoy, and G. R. Satchler, Comments Nucl. Part. Phys. **22**, 77 (1996).
[4] S. Ohkubo and Y. Hirabayashi, J. Phys. G: Conf. Ser. **111**, 012014 (2008).
[5] Y. Hirabayashi and S. Ohkubo, Phys. Rev. C **88**, 014314 (2013).
[6] Th. Delbar, Gh. Gregoire, G. Paic, R. Ceuleneer, F. Michel, R. Vanderpoorten, A. Budzanowski, H. Dabrowski, L. Freindl, K. Grotowski, S. Micek, R. Planeta, A. Strzalkowski, and K. A. Eberhard, Phys. Rev. C **18**, 1237 (1978).
[7] F. Michel and R. Vanderpoorten, Phys. Rev. C **16**, 142 (1977).
[8] F. Michel, S. Ohkubo, and G. Reidemeister, Prog. Theor. Phys. Suppl. **132**, 7 (1998).
[9] S. K. Kauffmann, Z. Phys. A **282**, 163 (1977).
[10] Yu. A. Berezhnoy and V. V. Pilipenko, Mod. Phys. Lett. A **10**, 2305 (1995).
[11] Yu. A. Berezhnoy and A. S. Molev, Int. J. Mod. Phys. E **12**, 827 (2003).
[12] A. A. Cowley and G. Heymann, Nucl. Phys. A **146**, 465 (1970).
[13] K. W. McVoy, Phys. Rev. C **3**, 1104 (1971).
[14] A. V. Kuznichenko, G. M. Onyshchenko, V. V. Pilipenko, N. Burtebayev, and G. S. Zhurynbaeva, Phys. At. Nucl. **70**, 1036 (2007).
[15] M. C. Mermaz, Phys. Rev. C **27**, 2019 (1983).
[16] F. Michel and G. Reidemeister, Phys. Rev. C **29**, 1928 (1984).
[17] H. M. Khalil, K. W. McVoy, and M. M. Shalaby, Nucl. Phys. A **455**, 100 (1986).
[18] K. W. McVoy, H. M. Khalil, M. M. Shalaby, and G. R. Satchler, Nucl. Phys. A **455**, 118 (1986).
[19] I. Jamir, E. F. P. Lyngdoh, and C. S. Shastry, Phys. Rev. C **57**, 1000 (1998).
[20] F. Michel and S. Ohkubo, Phys. Rev. C **70**, 044609 (2004).
[21] V. Yu. Korda, A. S. Molev, and L. P. Korda, Phys. Rev. C **72**, 014611 (2005).
[22] V. Yu. Korda, A. S. Molev, L. P. Korda, and V. F. Klepikov, Phys. Rev. C **79**, 024601 (2009).
[23] V. Yu. Korda, A. S. Molev, and L. P. Korda, Phys. At. Nucl. **72**, 1754 (2009).
[24] H. Löhner, H. Eickhoff, D. Frekers, G. Gaul, K. Poppensieker, R. Santo, A. G. Drentje, and L. W. Put, Z. Phys. A **286**, 99 (1978).
[25] H. H. Chang, B. W. Ridley, T. H. Braid, T. W. Conlon, E. F. Gibson, and N. S. P. King, Nucl. Phys. A **270**, 413 (1976).
[26] H. P. Gubler, U. Kiebele, H. O. Meyer, G. R. Plattner, and I. Sick, Phys. Lett. B **74**, 202 (1978); Nucl. Phys. A **351**, 29 (1981).
[27] V. Yu. Korda, S. V. Berezovsky, A. S. Molev, V. F. Klepikov, and L. P. Korda, Int. J. Mod. Phys. C **24**, 1350009 (2013).
[28] D. Agassi and N. S. Wall, Phys. Rev. C **7**, 1368 (1973).
[29] W. von Oertzen and H. G. Bohlen, Phys. Rep. **19**, 1 (1975).
[30] R. C. Fuller, Phys. Rev. C **12**, 1561 (1975).
[31] A. A. Ogloblin, S. A. Goncharov, Yu. A. Glukhov, A. S. Dem'yanova, M. V. Rozhkov, V. P. Rudakov, and W. H. Trzaska, Phys. At. Nucl. **66**, 1478 (2003).
[32] S. A. Goncharov, Yu. A. Glukhov, A. S. Dem'yanova, A. A. Ogloblin, M. V. Rozhkov, and W. Trzaska, Izv. Ross. Acad. Nauk, Ser. Fiz. **67**, 72 (2003).
[33] A. S. Demyanova, S. E. Belov, Yu. A. Glukhov, S. A. Goncharov, A. Izadpanakh, S. V. Khlebnikov, V. A. Maslov, Yu. G. Sobolev, A. A. Ogloblin, Yu. E. Penionzhkevich, W. H. Trzaska, A. Yu. Tultsev, and G. P. Tyurin, Phys. At. Nucl. **69**, 1383 (2006).
[34] M. E. Brandan and K. W. McVoy, Phys. Rev. C **43**, 1140 (1991).
[35] S. H. Fricke and K. W. McVoy, Nucl. Phys. A **467**, 291 (1987).
[36] M. E. Brandan, K. W. McVoy, and G. R. Satchler, Phys. Lett. B **281**, 185 (1992).
[37] K. W. McVoy, Nucl. Phys. A **455**, 141 (1986).
[38] G. Gaul, H. Lüdecke, R. Santo, H. Schmeing, and R. Stock, Nucl. Phys. A **137**, 177 (1969).
[39] Y. Kondo, S. Nagata, S. Ohkubo, and O. Tanimura, Prog. Theor. Phys. **53**, 1006 (1975).

[40] N. Takigawa and S. Y. Lee, Nucl. Phys. A **292**, 173 (1977).
[41] S. Y. Lee, N. Takigawa, and C. Marty, Nucl. Phys. A **308**, 161 (1978).
[42] W. E. Frahn, M. S. Hussein, L. F. Canto, and R. Donangelo, Nucl. Phys. A **369**, 166 (1981).
[43] D. M. Brink and N. Takigawa, Nucl. Phys. A **279**, 159 (1977).
[44] S. Ohkubo, Phys. Rev. C **38**, 2377 (1988).
[45] F. Brau, F. Michel, and G. Reidemeister, Phys. Rev. C **57**, 1386 (1998).
[46] S. Ohkubo, Phys. Rev. C **36**, 551 (1987).